doi:10.1016/j.jmb.2005.08.068 J. Mol. Biol. (2005) 353, 788–803

JMB

Available online at www.sciencedirect.com

SCIENCE DIRECT®

ELSEVIER

Structural Basis for the Voltage-gated Na^+ Channel Selectivity of the Scorpion α-Like Toxin BmK M1

Xiang Ye[1]†, Frank Bosmans[2]†, Chong Li[1], Ying Zhang[1] Da-Cheng Wang[1]* and Jan Tytgat[2]*

[1]*Center for Structural and Molecular Biology, Institute of Biophysics, Chinese Academy of Sciences, 15 Datun Road Beijing 100101, People's Republic of China*

[2]*Laboratory of Toxicology University of Leuven, E. Van Evenstraat 4, B-3000 Leuven Belgium*

**Corresponding authors*

Scorpion α-like toxins are proteins that act on mammalian and insect voltage-gated Na^+ channels. Therefore, these toxins constitute an excellent target for examining the foundations that underlie their target specificity. With this motive we dissected the role of six critical amino acids located in the five-residue reverse turn (RT) and C-tail (CT) of the scorpion α-like toxin BmK M1. These residues were individually substituted resulting in 11 mutants and were subjected to a bioassay on mice, an electrophysiological characterization on three cloned voltage-gated Na^+ channels ($Na_v1.2$, $Na_v1.5$ and para), a CD analysis and X-ray crystallography. The results reveal two molecular sites, a couplet of residues (8-9) in the RT and a hydrophobic surface consisting of residues 57 and 59–61 in the CT, where the substitution with specific residues can redirect the α-like characteristics of BmK M1 to either total insect or much higher mammal specificity. Crystal structures reveal that the pharmacological ramification of these mutants is accompanied by the reshaping of the 3D structure surrounding position 8. Furthermore, our results also reveal that residues 57 and 59–61, located at the CT, enclose the critical residue 58 in order to form a hydrophobic "gasket". Mutants of BmK M1 that interrupt this hydrophobic surface significantly gain insect selectivity.

Keywords: BmK M1; voltage-gated Na^+ channel; selectivity; α-like scorpion toxin

Introduction

Voltage-gated Na^+ channels (VGSCs) are transmembrane proteins responsible for the rising phase of action potentials in most excitable cells.[1–3] The central, pore-forming α-subunit of VGSCs consists of four homologous domains (260 kDa) and can be associated with up to four different auxiliary β-subunits (30–40 kDa). Until now nine mammalian ($Na_v1.1$–$Na_v1.9$) and three insect VGSCs have been cloned.[4,5] Despite their similarity in electrophysiology, primary structure and allocation of functional domains, the insect and vertebrate VGSCs are pharmacologically distinguishable.[6]

Since VGSCs play a pivotal physiological role, they constitute a target for toxins of various organisms. Up till now, nine different receptor sites have been described on the α-subunit.[7] The scorpion α-toxins, funnel web spider toxins and the sea anemone α-toxins all bind to site 3, resulting in delayed inactivation of the channel.[8–11] Here, we will focus on a toxin that interacts with this site.

According to their different pharmacological preferences, scorpion α-toxins can be divided into three subgroups: classical α; α-like; and insect α-toxins.[12,13] Classical α-toxins are highly toxic to mammals (e.g. AaH II) and insect α-toxins are toxic for insects (e.g. Lqh αIT).[14–16] α-Like toxins act on both mammals and insects, but do not bind to rat synaptosomes (e.g. BmK M1).[17–19] The molecular mechanism mediating such phylogenetic selectivity is a fundamental issue in understanding the structure–function relationship of scorpion toxins. Using the scorpion α-like toxin BmK M1 as a starting-point, we combined site-directed mutagenesis with electrophysiological tests on three cloned VGSCs expressed in *Xenopus laevis* oocytes

† X.Y. and F.B. contributed equally to this work.

Abbreviations used: VGSC, voltage-gated Na^+ channel; RT, reverse turn; CT, C-tail.

E-mail addresses of the corresponding authors: wangdcibp@yahoo.com.cn; jan.tytgat@pharm.kuleuven.be

($Na_v1.2$, $Na_v1.5$ and para) and X-ray crystallography in order to determine critical structural determinants for the pharmacological activity of this toxin.

BmK M1 is a scorpion α-like toxin from the eastern Asian scorpion *Buthus martensii* Karsch composed of 64 amino acid residues and cross-linked by four disulphide bridges.[17,19–25] Previous studies revealed three functionally important epitopes that underlie the molecular basis of mammal and/or insect-selectivity:[24,25] (1) the first three N-terminal residues; (2) the five-residue reverse turn (residues 8–12) in combination with the C-tail (residues 57–64); and (3) the loop between the β_1 and β_2 sheet (residues 40–43). The region consisting of the reverse turn (residues 8–12) in combination with the C-tail (57–64), previously termed "Site RC",[17] has received much attention due to its unique tertiary arrangement with an unusual non-proline *cis* peptide bond between residues 9 and 10.[17,26] Mutagenesis analysis revealed that this site is involved in the binding preference for phylogenetically distinct VGSCs.[24,25] A recent study from Karbat *et al.*[27] reported the transfer of these two motifs (here termed the NC-domain) of a scorpion α-insect toxin (LqhαIT) to the scaffold of the anti-mammalian scorpion α-toxin Aah II resulting in activity on insects.

Inspired by these studies, we further dissected the functional role of these critical residues in the NC-domain of BmK M1. As a result, 11 mutants of residues in the five-residue reverse turn (8–12) and C-tail (57–64) were thoroughly analysed. We found a molecular switch at position 8 (K8), where the substitution with specific residues can redirect the α-like characteristics of BmK M1 to either insect specificity or much higher mammalian specificity. 3D structures of the new mutants together with previously published data (K8D and K8Q[17,26]) reveal the structural mechanism which governs this molecular switch. In addition, the significance of the C-terminal residues 57 and 59–61, which form a hydrophobic "gasket" shielding the critical residue Arg58, has also been explored. As a result, we succeeded in pinpointing which residues are crucial for the selectivity of scorpion α-like toxins towards VGSCs. Remarkably, the mutation of one residue can completely alter the selectivity of BmK M1.

Results

Mutation, expression and purification

The expression levels of all mutants are displayed in Table 1. The Tricine/SDS/polyacrylamide gels and the mass spectra showed a high purity of the final products after purification with chromatography (data not shown). The molecular masses of all the mutants measured by ESI mass spectrometry are in agreement with their respective theoretical values (data not shown).

Bioassay

The mice showed typical symptoms of envenomenation after injection with rBmK M1. The LD_{50} value of unmodified rBmK M1 was ∼0.53 mg/kg, which is consistent with that of native BmK M1. The LD_{50} values of the mutants are listed in Table 1. K8D, K8D-P9S-R58K, K8D-P9S-H10V-R58K, K8D-P9S-R58K-V59G and K8D-P9S-R58K-P60G show no detectable toxicity even at a dose of 25 mg/kg, which is about 47 times the LD_{50} of rBmK M1. Mutants K8D/P9S, K8G, R58K and R58/P60G lose their toxicity significantly (only about 2.3%, 17%, 15% and 11% of BmK M1, respectively). K8A retains substantial toxicity (42%). K8Q displays a similar toxicity as rBmK M1 (106% of rBmK M1).[17,26]

Table 1. Overview of the data of rBmK M1 and mutants on mice and overview of the EC_{50} values obtained on $Na_v1.5/\beta_1$ (A) and para/tipE (B) expressed in *Xenopus laevis* oocytes

	Bioassay on mice			Bioassay on *X. laevis* oocytes		
Toxin/mutant	Expression (mg/l)	LD_{50} (mg/kg)	Rel. toxicity	EC_{50} $Na_v1.5/\beta_1$ (A) (nM)	EC_{50} para/tipE (B) (nM)	(A)/(B)
rBmK M1	3	0.53	100	500±30	30±6	16.7→100
K8A	7	1.3	42	–	24±9	*
K8D[17,26]	10	>25	<2	–	390±80	*
K8D/P9S	3	23	2	3800±300	220±200	1.7→10
K8G	3	3.07	17	–	32±20	*
K8Q[17,26]	6	0.50	106	1400±200	6200±600	0.2→1
K8D/P9S/R58K	3	>25	<2	–	–	–
K8D/P9S/R58K/P60G	3	>25	<2	–	–	–
K8D/P9S/R58K/V59G	3	>25	<2	–	549±42	*
K8D/P9S/H10V/R58K	3	>25	<2	–	–	–
R58K	16	3.6	15	740±40	47±21	15.7→94
R58K/P60G	3	4.9	11	–	3700±400	*

Each EC_{50} value is the result of measurements (≥6 different concentrations per oocyte) on at least three oocytes ($n \geq 3$) and is presented as the mean ±s.e.m. (A)/(B) for rBmK M1 is set to 100 as a reference. Values below 100 indicate an increased preference for $Na_v1.5/\beta_1$ and values above 100 indicate para/tipE selectivity. An asterisk (*) represents total insect selectivity.

Effect of BmK M1 and mutants on VGSCs

As a reference for the mutants, the reader is referred to published work[25] in which the maximum efficacy of rBmK M1 on the mammalian brain VGSC $Na_v1.2/\beta_1$ (5 μM), the mammalian heart VGSC $Na_v1.5/\beta_1$ (2 μM) and the neuronal insect VGSC para/tipE (500 nM) is displayed. Current traces recorded after the addition of rBmK M1 reveal a slowing of the inactivation process of the VGSCs studied. In order to present clearly the effect of the mutants on the three VGSCs studied, a topological way of presentation was chosen (Figures 1 and 2). This Figure displays the maximum efficacy of rBmK M1 and its mutants on $Na_v1.2/\beta_1$ (left traces) at a concentration of 5 μM, $Na_v1.5/\beta_1$ (middle traces) and para/tipE (right traces) at a concentration whereby the maximum effect was reached. Currents shown are the result of a two-electrode voltage clamp experiment on VGSCs expressed together with their β subunit (tipE for para) in *X. laevis* oocytes. Figure 2 reveals that K8D/P9S/R58K, K8D/P9S/R58K/P60G and K8D/P9S/H10V/R58K do not affect the VGSCs studied anymore at concentrations up to 20 μM. K8D, K8A, K8G, R58K/p60G and K8D/P9S/R58K/V59G only affect para/tipE at concentrations up to 1 μM, indicating their insect specificity. A very small effect on $Na_v1.5/\beta_1$ at high concentrations (up to 20 μM) is seen for mutants K8A and K8G. K8Q affects both $Na_v1.5/\beta_1$ and para/tipE but at different concentrations (Table 1). R58K still affects $Na_v1.5/\beta_1$ and para/tipE equal to BmK M1. Except for a certain efficacy of R58K/P60G, none of the other mutants had an effect on $Na_v1.2/\beta_1$.

The slowing of inactivation induced by rBmK M1 and its mutants is concentration-dependent (Table 1). The EC_{50} values were determined according to published procedures.[25] EC_{50} values of rBmK M1 and its mutants on $Na_v1.2/\beta_1$ were not determined, since rBmK M1 had only a small effect on this VGSC at high concentrations (5 μM). The EC_{50} values on $Na_v1.5/\beta_1$ (A) are divided by the ones from para/tipE (B) and represented in the final column of Table 1. All results were normalized to BmK M1 ((A)/(B)=100). Mutant values (A)/(B) below 100 indicate an increased preference for $Na_v1.5/\beta_1$ (mammal); (A)/(B) values above 100 indicate an increased preference for para/tipE (insect). The asterisk (*) indicates the total insect specificity. K8Q has significantly gained selectivity towards $Na_v1.5/\beta_1$. K8A, K8D, K8G, R58K/P60G and K8D/P9S/R58K/V59G have greatly increased their selectivity towards the insect VGSC, para/tipE. A general overview of the results regarding efficacy and potency of rBmK M1 and its mutants on $Na_v1.2/\beta_1$, $Na_v1.5/\beta_1$ and para/tipE referenced to rBmK M1, is presented as a bar diagram in Figure 3.

CD analysis

R58K, R58K/P60G and K58D/P9S/H10V/R58 were subjected to CD analysis (no crystal structure available). Compared to rBmK M1, the CD spectra of all mutants did not have a significant change, indicating that these mutations do not alter the general secondary structure of the toxin (data not shown).

3D structure of the mutants

Among the 11 mutants of six residues situated in the NC-domain, eight crystal structures were determined at high resolutions from 1.30 Å to 1.85 Å. Analysis of the stereochemistry shows that all geometric parameters are within the limits expected for the resolutions of these structures.

Mutated residues can be clearly distinguished by either $2F_o-F_c$ or omit F_o-F_c maps for every mutant (see Figure 4(a)). The structural superimposition (see Figure 4(b)) shows that the general structures of these mutants were not altered, but certain local structural changes subtly appeared near the mutation position, namely residue 8. The stereochemical statistics of the final models are provided in Table 2.

Unique conformational states induced by mutating residue 8

Position 8 in the native sequence of BmK M1 is occupied by a long-chain basic residue, lysine, which protrudes from the five-residue reverse turn (8–12) and is fully exposed to the solvent. The flanking peptide bond (9–10) adopts an unusual *cis* form (Figure 5).[17,26] 3D structures of the five mutants at residue 8 reveal three distinct conformational states around this residue, which correspond to the three pharmacological properties induced by these mutations. In BmK M1 itself, the surface at position 8 is bulgy and positively charged. In mutant K8D,[17,26] which is totally insect-specific, the shape of the surface becomes flat and is negatively charged (Figure 5(a)). The crystal structure reveals that the rather long side-chain of Asp8 has been bent into the five-residue turn (8–12). This unique conformational state is mediated by the *cis* to *trans* conversion of the peptide bond (9–10) flanking residue 8. This can be seen in the structure of mutant K8D at a resolution of 1.5 Å. Correspondingly, both the side-chain of Asp8 and the main-chain N atom of His10 are rotated into the reverse turn as compared to BmK M1. These changes induced by Asp8 force the reverse turn to adopt a new conformational state, in which the $O^{\delta1}$ atom of Asp8 makes contact with the backbone N atoms of residues 10 and 12 to form a couple of tight hydrogen bonds ("fireman's grip"). As a consequence, Asp8 leaves only atom $O^{\delta2}$ on the surface of the molecule (Figure 5(b)). Furthermore, this conformational transition also results in the abolishment of contacts between the peptide bond 9–10 and the C-terminal residues, saving only a single hydrogen bond between the main-chain atoms of residues His10 and His64 (Figure 5).

The second conformational state around position

Table 2. Statistics of X-ray data and model qualities for the mutant structures of BmK M1

	K8D	K8A	K8Q	K8G	K8D-P9S	K8D-P9S-R58K	K8D-P9S-R58K-V59G	K8D-P9S-R58K-P60G
A. *Data quality*								
Space group	$P2_12_12$	$P2_12_12$	$P2_12_12$	$P2_12_12$	$P2_12_12$	$P2_12_12$	$P2_12_12$	$P2_12_12$
Unit-cell dimensions								
a (Å)	47.45	47.24	47.59	46.85	47.40	47.10	47.36	46.86
b (Å)	44.34	43.07	44.06	42.65	44.34	43.32	43.87	43.54
c (Å)	25.49	25.46	25.51	25.24	25.45	25.42	25.52	25.43
α, β, γ (deg.)	90, 90, 90	90, 90, 90	90, 90, 90	90, 90, 90	90, 90, 90	90, 90, 90	90, 90, 90	90, 90, 90
Resolution range (Å)								
Overall	30.0-1.50	31.8-1.33	30.0-1.85	31.5-1.70	23.7-1.20	31.9-1.70	22.5-1.50	22.4-1.30
Highest resolution shell	1.55-1.50	1.41-1.33	1.92-1.85	1.81-1.70	1.28-1.20	1.81-1.70	1.59-1.50	1.38-1.30
No. observations	41,017	25,535	28,173	23,164	66,285	18,250	57,018	92,623
No. unique reflections	8946	9550	4831	5890	15,517	5420	8962	13,231
Completeness (%)[a]	98.1(93.3)	77.0(41.3)	97.6(93.8)	99.1(97.6)	89.0(58.4)	88.7(75.2)	99.0(100.0)	99.0(99.1)
R_{merge} (%)[a]	5.2 (17.5)	4.15(11.6)	8.3(28.3)	5.1(14.6)	5.0(27.5)	7.4(41.5)	4.1(9.8)	5.1(15.2)
$I/\sigma(I)$	28.3(8.7)	12.3(3.5)	22.0(6.0)	10.0(4.6)	23.2(3.2)	7.0(1.5)	10.0(7.1)	9.2(4.2)
R_{work} (%)	0.165	0.169	0.171	0.186	0.158	0.203	0.170	0.143
R_{free} (%)	0.183	0.190	0.197	0.223	0.164	0.229	0.198	0.171
B. *Model quality*								
B-factors								
Wilson ($Å^2$)	17.5	8.0	19.8	15.2	7.4	12.7	10.3	7.8
Protein ($Å^2$)	10.4	11.8	17.5	11.8	9.0	16.0	11.6	8.9
Water ($Å^2$)	27.5	25.0	30.3	25.1	27.5	27.0	26.0	25.8
Other ion groups ($Å^2$)	/	/	/	14.0	/	22.5	/	18.2
RMS deviations								
Bond lengths (Å)	0.004	0.012	0.008	0.005	0.006	0.009	0.004	0.018
Bond angles (deg.)	1.300	1.670	1.550	1.400	1.361	1.500	1.200	1.800
Ramachandran plot								
Core regions (%)	92.6	90.3	90.7	90.6	94.5	90.9	88.9	89.1
Additional allowed regions (%)	7.4	9.7	9.3	9.4	5.5	9.1	11.1	10.9

[a] Values for the highest resolution shell are given in parentheses.

8 induced by mutations K8A and K8G results in a flat surface with hydrophobic properties. Pharmacologically, K8A and K8G have gained insect specificity but still display a certain effect on mammalian VGSCs (Table 1). In this case, the peptide bond between residues 9 and 10 is still in *cis* conformation. Evidently, the shortening (K8A) or removal (K8G) of the side-chains accounts for the flat shapes at this position (Figure 5).

In contrast to mutant K8D, the mutation K8Q results in the retention of the *cis* conformation of the peptide bond 9–10. Consequently, the orientation of the side-chain of glutamine (Gln) in the K8Q mutant is still protruding from the reverse turn and forms an extended bulgy shape on the molecule surface. This spatial topography is comparable to that of BmK M1, but the stereochemical properties at this position are different. This bulgy site at position 8 is polar uncharged in the K8Q mutant, while positively charged in BmK M1 (Figure 5). From the bioassays, it seems that K8Q has become more specific for the mammalian VGSC.

The structure of the K8D/P9S mutant reveals that the orientation of residue Asp8 and the geometry of the five-residue turn are almost the same as in mutant K8D. However, due to the P9S mutation, the hydrophobic prolinyl ring of Pro9 flanking Asp8 has changed to an exposed polar surface, which is formed by the OH group of Ser9 and the main-chain N and O atoms surrounding Ser9 (Figure 5). Correspondingly, mutant K8D/P9S displays a restored mammal specificity with a decreased potency towards the mammalian VGSC. As a consequence, residue 8 can be considered a "hot spot" for the binding preference of BmK M1. Furthermore, the small hydrophobic pocket formed by Pro9 is tightly linked in functional performance to the flanking Asp8 residue. In confirmation, a previous study showed that the P9S mutation resulted in changes of the potency of the toxin.[24]

Structures of the mutants of the C-tail

In order to analyse the structure–function relationship between the K8D mutation and the C-tail, mutant R58K and five other mutants containing K8D and R58K were constructed (Table 1). The structure of K8D/P9S/R58K, K8D/P9S/R58K/V59G and K8D/P9S/R58K/P60G was determined. Only some subtle conformational alterations were noticeable (Figure 6). In three mutants, the accessible areas of the functional group of residue 58 side-chain 8 are reduced due to the alteration of a guanido group in the native toxin (Arg58) to a NH_2 group in the mutants (Lys58). This leads to the conclusion that residue 58 is crucial for the

bioactivity.[24] Arg58 is situated in a cavity surrounded by the side-chains of Asn11, Thr13 and Tyr42, and is stabilized by several hydrogen bonds, including 58 N^{ε}…O 11 (2.96 Å), 58 $N^{\eta 1}$…O 59 (2.75 Å) and 58 $N^{\eta 1}$…O 61 (2.83 Å), which make the guanido group of the side-chain on the molecule surface accessible to ligands and in contact with the RT sector of the NC-domain (Figure 6). In three mutants containing the R58K mutation, the contact of 58 N^{ε}…O 11 is abolished and the above interactions of residue 58 with residues 59 and 61 are replaced by the contact between N^{ζ} of Lys58 and O61 (Figure 6). N^{ζ} is still ligand-accessible but the area is reduced. Also, the interaction between residue 58 and the RT is abolished. This could be the structural reason for the significant reduction of potency of mutant R58K and the extremely low potencies of other mutants with multiple mutations in this vicinity. Furthermore, substitutions of residues V59 and P60 by Gly have interrupted the hydrophobic gasket surrounded residue 58 at these positions (Figure 6). Interestingly, the mutants K8D/P9S/R58/V59G and R58K/P60G have increased their specificity greatly towards the insect VGSC, para/tipE (Table 1). The present observations show that the shielding by a hydrophobic surface of residue 58 is important for the preference of BmK M1 for distinct VGSCs.

Discussion

The molecular dissection of the interaction between scorpion toxins and one of their targets, VGSCs, has been an extensively pursued topic. Since the pioneering work of several researchers in the 1970s,[28–31] the availability of producing recombinant toxins and the cloning and expression of several subtypes of VGSCs has caused a significant progress in this field. Recently, the importance of the conserved aromatic residues in BmK M1 was investigated.[23] In this study it was demonstrated that Trp38 and Tyr42 are involved in the functional performance of the toxin and that the side-chains of residues Trp47, Tyr14 and Tyr35 are important for the structural stability of BmK M1. Tyr5 seems to be essential for the correct folding of the toxin. The clarification of the molecular determinants of mammalian VGSC binding of scorpion α-toxins has also been undertaken. In 2004, Benkhadir *et al*.[32] cloned and expressed the scorpion α-toxin BotIII and confirmed the pivotal role of the C-terminal region for its interaction with VGSCs. The importance of this region is also reported in other studies.[33] In the study by Benkhadir *et al*.[32] it is clearly shown that C-terminal amidation of BotIII plays an important role in toxin recognition of receptor site 3. Moreover, a single mutation of the C-terminal His64 instead of Asn64 also indicated the involvement of this residue in receptor binding. In this study, it was also reported that C-terminal carboxylation of AaH II (a scorpion α-toxin from *Androctonus australis* Hector) also decreases its potency on rat brain synaptosomes. In 2005, Legros *et al*.[34] expressed Aah II and some mutants in order to identify putative key bioactive elements. There it was stated that the lack of amidation on the C-terminal residue His64 does not affect the pharmacological activity of AaH II. Conversely, the replacement of Lys58 by a hydrophobic (Val and Ile) or acidic (Glu) amino acid residue immediately led to an inactive analogue, leading to the conclusion that this position is very important for the pharmacological function of this toxin family. Another study in 2005 confirmed the C-terminal region as being important for the target specificity of BmK M1.[25] Here, it was stated that there are three epitopes that determine the VGSC specificity of this toxin: (1) the first three N-terminal residues; (2) the five-residue turn (residues 8–12) in combination with the C-tail (residues 57–61); and (3) the loop between the β_2 and β_3 sheet including the adjacent Gly residue in the β_3 sheet (residues 40–43). These three domains were actually a fine-tuning of a previously reported hypothesis by Karbat *et al*.[27] In this study, the molecular basis of the high insecticidal potency of scorpion α-toxins was investigated by extensive mutagenesis[35] of the insect scorpion α-toxin LqhαIT. Consequently, two distinct domains of this toxin were transferred to AaH II (mammal-specific) resulting in insect activity of this toxin. These two domains consist of a conserved "core domain" formed by amino acids of the loops connecting the secondary structure elements of the molecule core and the C-terminal segment (residues 56–64).

Altogether, these studies point to the crucial role of the NC-domain in scorpion α-toxins and the interaction of this site with the C-tail, and in particular with the residue at position 58. For this reason, we investigated this region thoroughly in order to give a detailed and well motivated explanation about VGSC subtype specificity of the scorpion α-like toxin BmK M1.

A molecular switch for insect/mammal selectivity

Remarkably, in electrophysiological measurements on the three VGSCs studied, a single mutation at residue 8 can redirect the toxin to either total insect or much higher mammal specificity (Table 1 and Figure 3). When residue 8 is acidic and contains a proper side-chain geometry (Asp), or if the side-chain atoms are removed (Gly and Ala), the toxin displays a high degree of insect specificity. However, the substitution of residue 8 with a Gly or an Ala residue still induces a certain (lower) potency towards mammals. When a long-chain residue with an amide group is present (Gln), the toxin is more mammal-specific with respect to BmK M1 (Table 1 and Figure 3). The wild-type basic residue Lys at position 8 represents a third outcome of the molecular switch: the α-like characteristics of BmK M1.

The structure–function analysis of the mutant

K8D/P9S, as described above, has indicated that residues 8 and 9 are linked as a unity in functional performance (see Results). In fact, in all sequences of α-like toxins reported so far, residue Pro9 is invariable (see Figure 1). Thus, the couplet of residues (8-9) can be considered as a molecular switch for the pharmacological preference of BmK M1 for insect/mammalVGSCs. In this couplet, residue 8 serves as a hot spot. In BmK M1 itself, the consensus sequence Asp8-Pro9, Gln8-Pro9 and Lys8-Pro9, respectively, corresponds to preferences for insect, highly mammal, and both insect and mammal VGSCs. Sequence alignment of α-like toxins (Figure 1) shows that the residue couplet (9-10) appears as Lys8-Pro9 or Gln8-Pro9 in the native toxins conservatively. In fact, this molecular switch may also relate to the general fold of the toxin, since our attempts to express BmK M1 mutants with similar amino acid substitutes at position 8, including Glu (K8E) and Asn (K8N), have failed. This suggests a possibility that these mutants may represent a particular outcome of the molecular switch, which results in a local structure that is incompatible with the global folding of the toxin molecule.

3D structural comparisons of the mutants reveal that the biological ramification described above is accompanied by the reshaping of the surface around residue 8. In the native BmK M1, the side-chain of Lys8 protrudes from the five-residue reverse turn in order to form a positively charged bulged surface. In sharp contrast, in mutant K8D

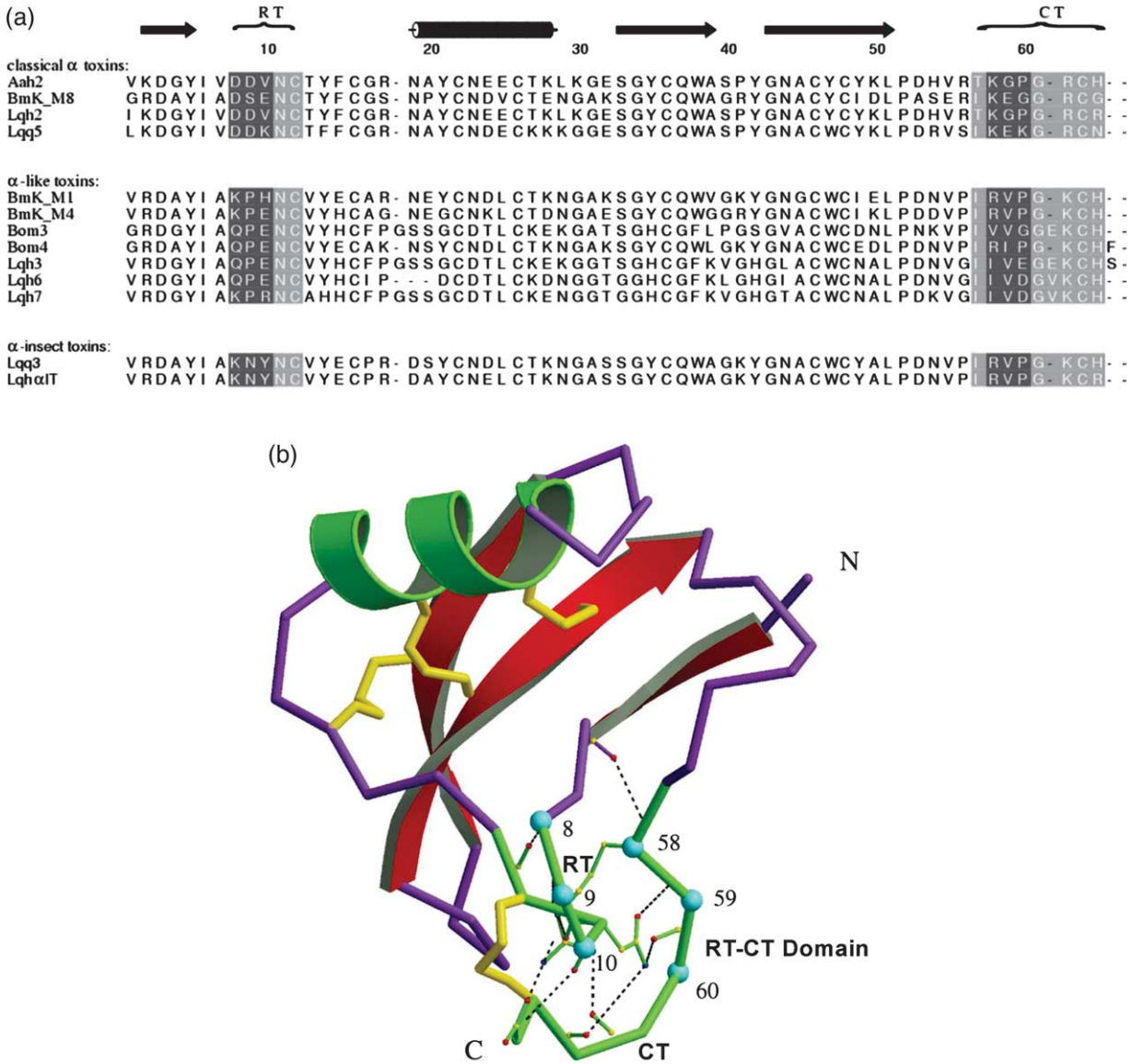

Figure 1. Location of the residues selected for mutagenesis on (a) the sequence and (b) 3D structure of BmK M1. (a) Comparison of the amino acid sequences of different subgroups of scorpion α-toxins.[8] Secondary structure elements are denoted on top of the sequences. Residues of the five-residue reverse turn (8–12) (RT) and C-tail (57–64) (CT) are shaded, while the mutated residues from this work are in black-white. (b) Schematic view of the BmK M1 with selected mutation sites (cyan-coloured spheres) in the reverse turn 8–12 and C-terminal segment 57–64.

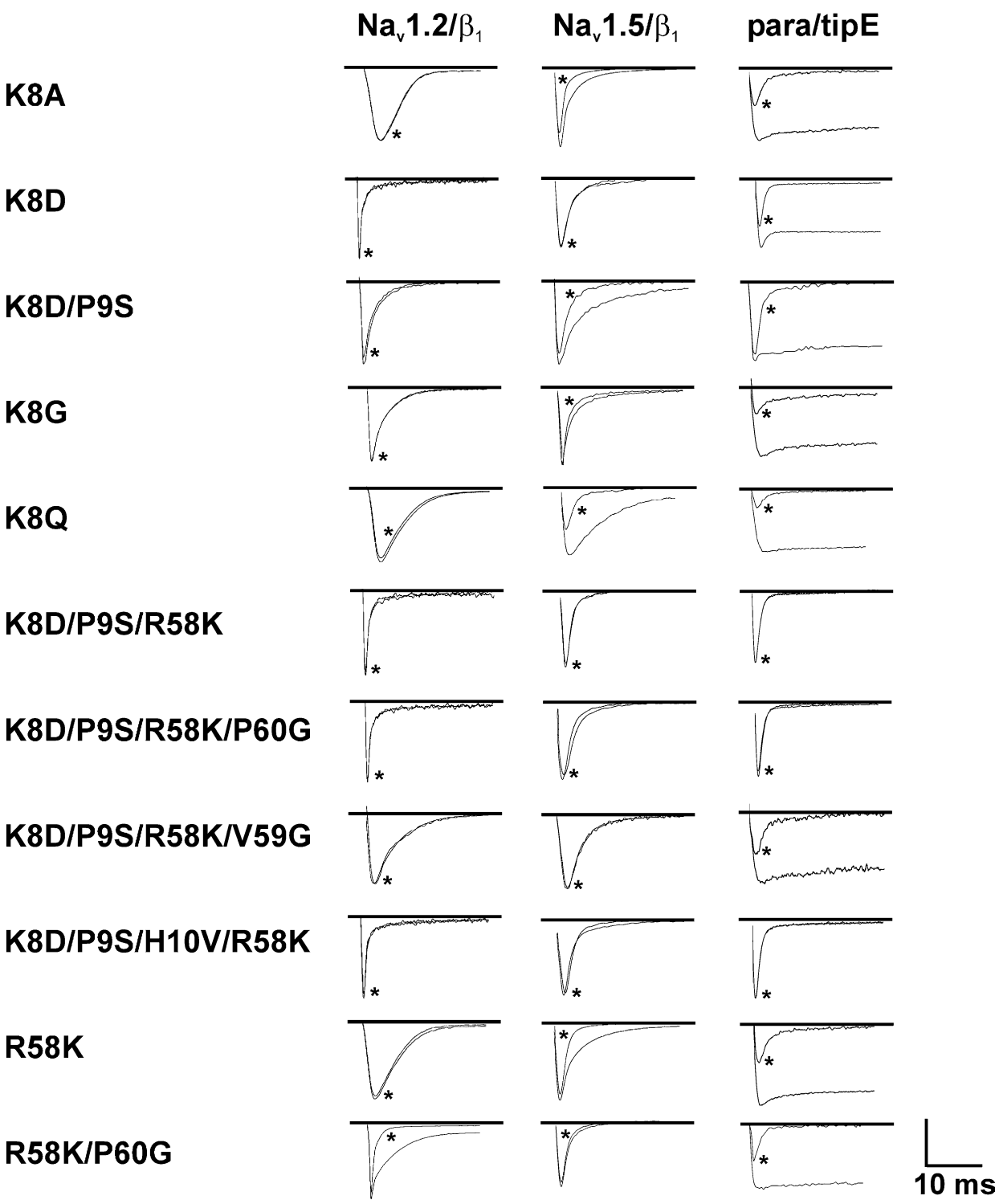

Figure 2. Effect of rBmK M1 mutants on the inactivation kinetics of Na$_v$1.2/β_1, Na$_v$1.5/β_1 and para/tipE expressed in *X. laevis* oocytes. Current traces were evoked by depolarisations ranging from −20 to 10 mV, depending on the VGSC, from a holding potential of −90 mV. All concentrations shown for Na$_v$1.2/β_1 are 5 μM. Concentration of mutants shown for Na$_v$1.5/β_1 are 20 μM except for K8Q and R58K which are 5 μM. Concentration of mutants shown for para/tipE are: 1 μM for K8G, K8A and R58K; 2 μM for K8D and K8D/P9S/R58K/V59G; 5 μM for K8D/P9S; 10 μM for R58K/P60G; 20 μM for K8Q, K8D/P9S/R58K, K8D/P9S/R58K/P60G and K8D/P9S/H10V/R58K. The scale-bare *Y*-axis for all mutants represents about 0.5 μA for Na$_v$1.2/β_1, 1.5 μA for Na$_v$1.5/β_1 and 0.4 μA for para/tipE. The asterisk (*) indicates control conditions where no toxin was added.

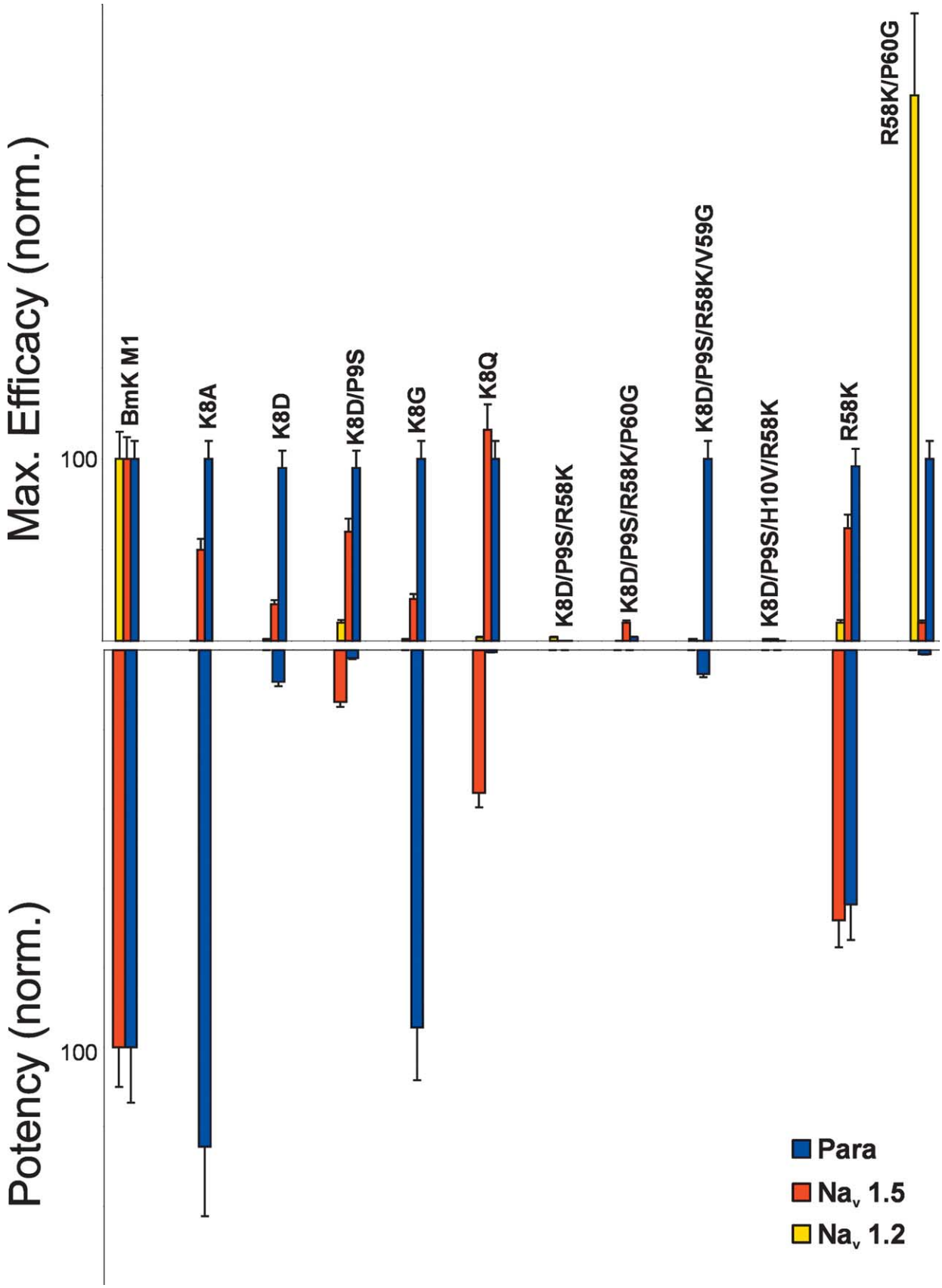

Figure 3. Bar diagram representing the maximum efficacies (upper panel) of the mutants studied referenced to rBmK M1 (100) on $Na_v1.2/\beta_1$ (yellow), $Na_v1.5/\beta_1$ (red) and para/tipE (blue). The lower panel shows the potencies obtained after sigmoidal fit of the data on $Na_v1.5/\beta_1$ and para/tipE referenced to rBmK M1. All data represent the mean $\pm$S.E.M ($n \geq 3$).

the surface around residue 8 has changed to a negatively charged flat topography (Figure 5). In this case, the aspartic side-chain of residue 8 bends into the five-residue reverse turn leaving only the functional atom $O^{\delta 2}$ atom exposed on the molecular surface (Figure 5). This negatively charged flat conformational state surrounding residue 8 appears to be the structural basis for the insect specificity of the toxin. Similarly, in mutants K8G and K8A the corresponding surfaces also become flat due to lack of the side-chain, but here they are hydrophobic (Figure 5). In this case, both mutants seem to be more potent towards the insect VGSC with certain residual effects on $Na_v1.5$ and mice (Table 1 and Figure 3). These observations support the point of view that the flat topography of residue 8 is required for the insect specificity, but further indicate that the appropriate stereochemical property of this surface is also significant. In sharp contrast to K8D, residue Gln8 in mutant K8Q adopts another conformational state. This polar uncharged side-chain with an amide group is protruding from the five-residue reverse turn in order to form a polar uncharged bulgy surface around residue 8 (Figure 5). In this case the toxin is more mammal-specific with respect to BmK M1 (Table 1; Figures 2 and 3).

The structural mechanism mediating the molecular switch

Comparison of the new mutant structures in this study and two structures from a previous study[17,26] reveals that the distinct conformational states of residue 8 towards insect/mammal VGSCs are mediated by the *cis*/*trans* isomerization of the peptide bond between residues 9 and 10. In contrast to the crystal structure of BmK M1,[17] mutant K8D clearly reveals that the *cis* peptide bond between residues 9 and 10 is dramatically converted into the *trans* conformation (Figures 4 and 5). Correspondingly, both $2F_o-F_c$ and F_o-F_c electron density maps show that the C^α atoms of residues 9 and 10 in K8D are located on opposite sides of the 9–10

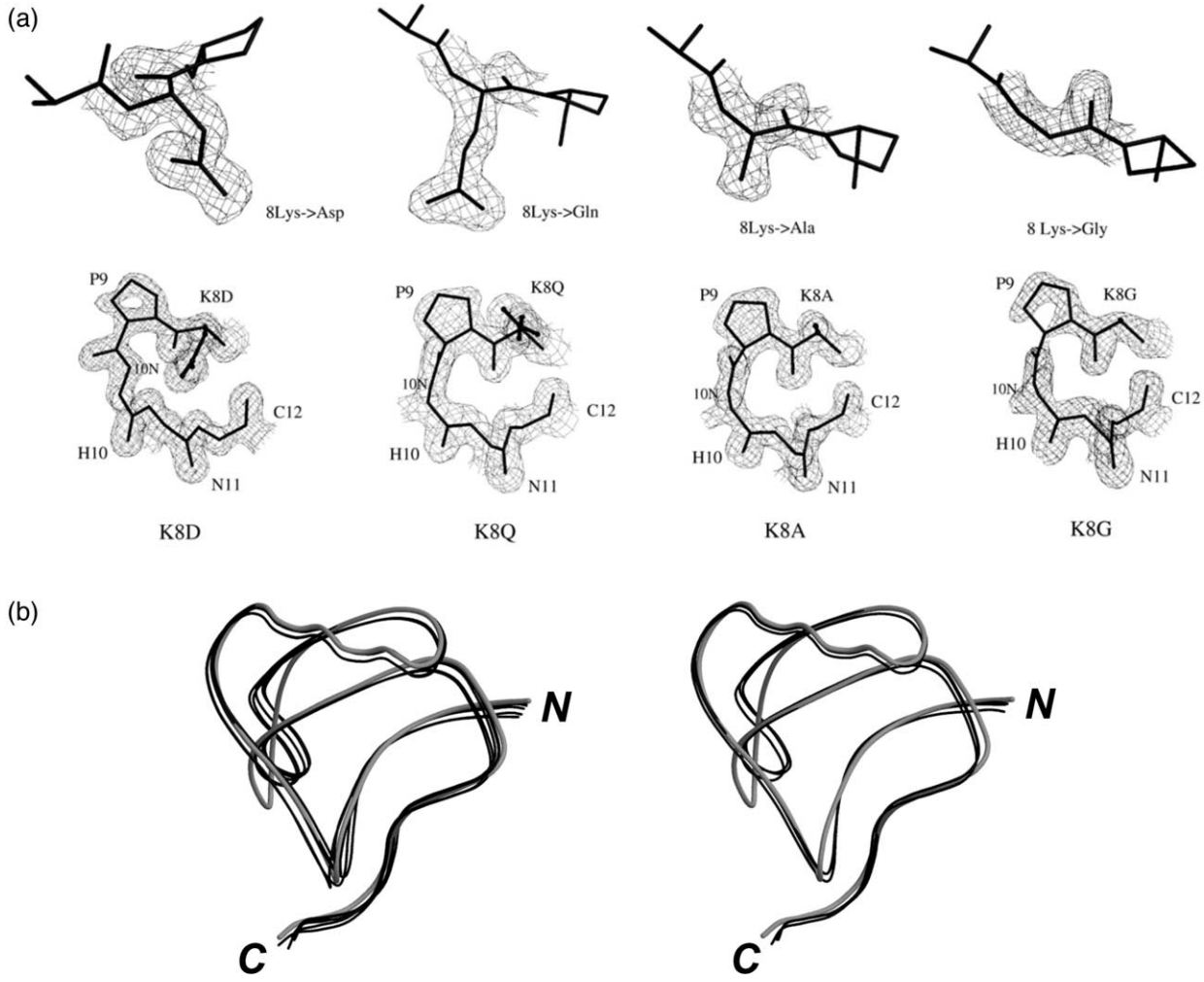

Figure 4. (a) Electron density maps around the mutated residues at position 8 (up) (omit F_o-F_c maps, contoured at 3.0σ) and the reverse turn (8–12) in different conformational states with *trans* peptide bond 9–10 (K8D) and *cis* peptide bond 9–10 (K8Q, K8A and K8G) (down) ($2F_o-F_c$ maps contoured at 1.0σ). (b) Main-chain trace superimposition of eight mutant structures.

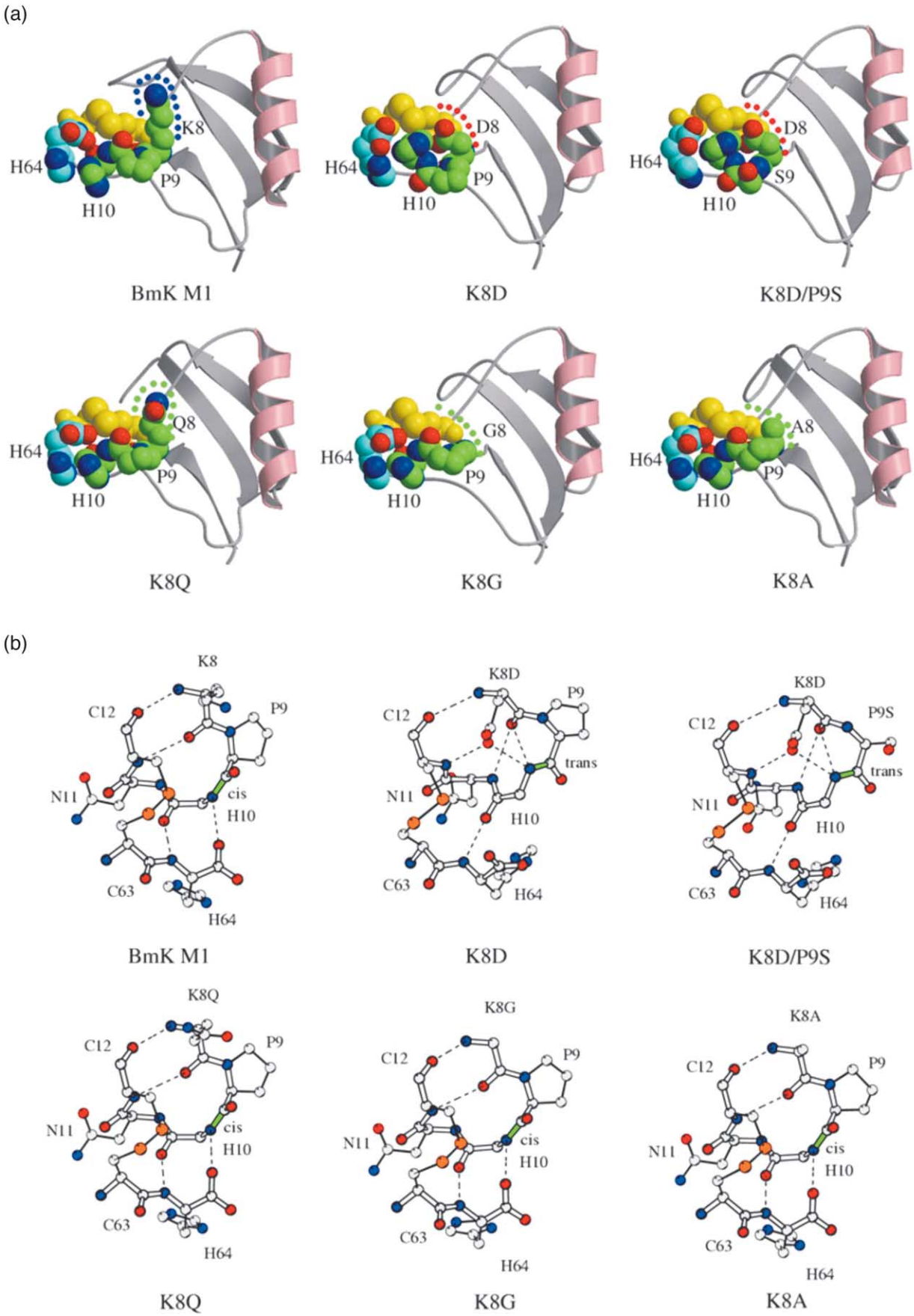

Figure 5 (*legend opposite*)

peptide bonds (Figure 4(a)). Accompanying the *cis*/*trans* conversion, both the N main-chain atom of His10 and the side-chain of Asp8 are rotated into the reverse turn causing a new, flat conformational state with acidic properties (Figure 5(b)). However, in mutants K8Q and BmK M1, peptide bond 9–10 adopts the unusual *cis* conformation (Figures 4(a) and 5(b)) resulting in a protrusion of the side-chain from the reverse turn (Figure 5). Furthermore, mutants K8G and K8A reveal another approach to achieve the flat surface, namely by removing the side-chain (e.g. Gly, Ala). In this case, there is no peptide reconfiguration and the peptide bond (9–10) is still in the *cis* form.

Role of C-tail residues in promoting insect selectivity

R58K[13,24,25,27] is the only mutant in this study that still affects all three VGSCs studied but with a large reduction of toxicity towards mice (Table 1 and Figure 3). In the native BmK M1 structure, Arg58 is situated in a subtle tertiary arrangement.[17] Its side-chain is located in a cavity surrounded by the conserved residues Asn11, Val13 and Tyr42, and makes tight contacts with the main-chain CO group of Asn11 belonging to the five-residue (8–12) reverse turn. Moreover, residue 58 is rooted on a string of conserved hydrophobic residues, including Ile57, Val59, Pro60 and Gly61, which form a hydrophobic gasket for shielding residue 58 from solvents (Figure 6). As a consequence, the critical residue 58 is linked to both the RT sector, on the one hand, and the CT sector, on the other hand. In order to investigate the relationship between these two sectors in the RT–CT domain, five multiple mutations were constructed. K8D/P9S/R58, K8D/P9S/R58K/P60G and K8D/P9S/R58K/H10V show no effect at all on the VGSCs studied. Considering both K8D/P9S and R58K are active on $Na_v1.5$ and para/tipE, the results indicate that the preference of the toxin for VGSCs requires the contribution of both sectors of the RT–CT domain. The crystal structures of K8D/P9S/R58K and K8D/P9S/R58K/P60G show that the contact between residue 11 and residue 58 has been destroyed (Figure 6). The cooperative conformational change of the RT–CT domain may be one of the structural factors for the loss of the pharmacological potency of these mutants.

Mutants R58K/P60G and K8D/P9S/R58K/V59G have become insect-specific (Figure 3 and Table 1), which indicates that residues 59 and 60 are involved in VGSC selectivity. The crystal structure of K8D/P9S/R58K/V59G shows that the general structure is similar to that of K8D/P9S/R58K, but the hydrophobic gasket of residue 58 was interrupted at position 59 by the V59G mutation (Figure 6). In the crystal structure of K8D/P9S/R58K/P60G (Figure 6), the hydrophobic gasket is interrupted at position 60 due to the mutation of proline to a glycine. We hypothesize that there will be a similar surface disturbance at residue 60 in mutant R58K/P60G. Therefore, the insect selectivity gained from mutation R58K/P60G can also be attributed to the same structural reason. In a previous study,[25] the single mutations of I57G and G61A had also gained insect selectivity significantly. All these results indicate that the C-tail residues 57 and 59–61, being the hydrophobic gasket for residue 58, are also essential for the insect/mammal selectivity of BmK M1 for VGSCs.

In conclusion, two molecular sites, a couplet of residues (8-9) and a hydrophobic surface consisting of residues 57 and 59–61, have been found to be important for the pharmacological preference of BmK M1 for insect or mammalian VGSCs. The residue couplet (8-9) is situated at the RT sector of the RT–CT domain (i.e. the NC-domain according to Karbat *et al*.[27]) and acts as a molecular switch, where the substitution at position 8 with specific residues can redirect the α-like characteristics of BmK M1 to either total insect or much higher specificity. The residue 57 and 59–61 located at the CT sector of RT–CT domain enclose the critical residue 58 as a hydrophobic gasket. Mutations that interrupt this hydrophobic surface at one of these positions cause a gain in insect selectivity.

Materials and Methods

Strains, materials and animals

Plasmid pVT102U/α, *Escherichia coli* strain TG1, and *Saccharomyces cerevisiae* strain S-78 (Leu2, Ura3, Rep4) were used for plasmid constructions. Restriction endonucleases were obtained from Promega (WI, USA). Taq DNA polymerase and the primers were obtained from Sangon (Shanghai, China). The bioassay was performed

Figure 5. (a) Conformational state surrounding residue 8 in different mutants and native BmK M1. Residues around position 8 including 8–12 and 63–64 are space-filled and coloured according to their chemical nature and locations (carbon atoms of residues 8–11 and residue 64 are green and cyan, respectively; nitrogen and oxygen atoms of these residues are in blue and red, respectively; two cysteine residues 12 and 63 are yellow). Broken lines with different colours highlight the surface of residue 8 (positive, blue; negative, red; neutral, green). (b) Distinct structures of the five-residue reverse turn (RT) in association with the C-tail (CT) of the mutants containing *trans* peptide bond 9–10 (K8D and K8D/P9S) and *cis* peptide bond 9–10 (K8Q, K8A and K8G). In the *trans*-containing form, the peptide group NH10 is situated inside the turn and residue 8 must be Asp, which interact with each other *via* hydrogen bond N10…$O^{\delta 1}$ 8. There is no contact between the NH10 group and the C-terminal residue, referred to as transRT-freeCT. In *cis*-containing form group NH10 points out of the reverse turn and interacts with the C-terminal residue *via* hydrogen bond N10…O64, referred to as cisRT-bondCT. The side-chain of H10 is not shown.

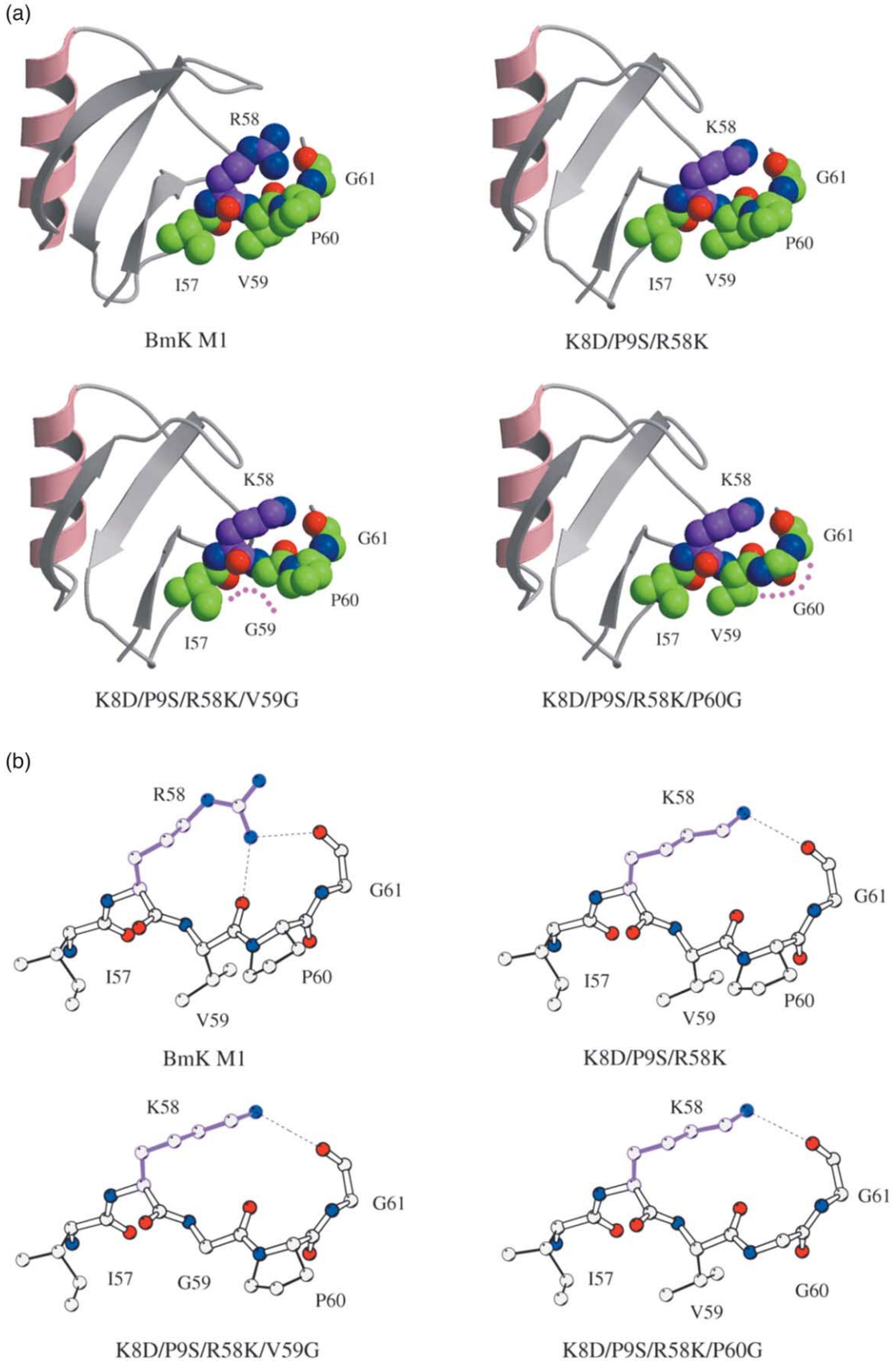

Figure 6. (a) Conformational states of C-tail residues 58–61 in three mutants relative to residue 58. Residues around position 58 are space-filled. Carbon atoms of residue 58 are in purple. Nitrogen atoms, oxygen atoms and carbon atoms of other residues are in blue, red and green, respectively. Surfaces at two mutated residues 59 and 60 are highlighted with purple broken lines. (b) Structures of the C-tail corresponding to the highlighted parts shown in (a).

on ICR mice from the Beijing Centre for Experimental Animals.

Site-directed mutagenesis of BmK M1

Five mutants containing residue 8 and six mutants from C-tail residues 58, 59 and 60 were constructed: K8D, K8A, K8G, K8Q, K8D/P9S, R58K, R58/P60G, K8D/P9S/R58K, K8D/P9S/R58K/P60G, K8D/P9S/R58K/V59G and K8D/P9S/H10Y/R58K. The cDNA of BmK M1 was cloned previously[21] and inserted into pVT102U/α.[22] All site-directed mutations of BmK M1 were introduced by one-step PCR with corresponding synthetic primers and pVT102U/α-BmK M1 (recombinant (r)BmK M1) or mutated pVT102U/α-BmK M1 expression vectors as templates. The location of the residues selected for mutagenesis is shown in Figure 1. According to the sequence of pVT102U/α, two primers were designed: primer 1 (5′-CGT CTA GAT AAA AGA AAT TCT GTT CGG-3′, including a KEX2 protease linker and an XbaI restriction site) and primer 2 (5′-CG AAG CTT TTA ATG GCA TTT TCC TGG TAC-3′, with a HindIII restriction site). Next, the mutagenic primers used to generate the desired mutations were designed as follows: K8D, 5′-CGT CTA GAT AAA AGA AAT TCT GTT CGG GAT GCT TAT ATT GCC **GAT** CCC CAT AAC-3′; K8G, 5′-CGT CTA GAT AAA AGA AAT TCT GTT CGG GAT GCT TAT ATT GCC **GGT** CCC CAT AAC-3′; K8A, 5′-CGT CTA GAT AAA AGA AAT TCT GTT CGG GAT GCT TAT ATT GCC **GCT** CCC CAT AAC-3′; K8Q, 5′-CGT CTA GAT AAA AGA AAT TCT GTT CGG GAT GCT TAT ATT GCC **CAA** CCC CAT AAC-3′; R58K, 5′-CG AAG CTT TTA ATG GCA TTT TCC TGG TAC **CTT** AAT CGG TAC-3′; K8D-P9S, 5′-CGT CTA GAT AAA AGA AAT TCT GTT CGG GAT GCT TAT ATT GCC **GAT AGT** CAT AAC-3′; R58K-P60G, 5′- CG AAG CTT TTA ATG GCA TTT TCC **GGT** TAC **CTT** AAT CGG TAC-3′; K8D-P9S-R58K, 5′-CG AAG CTT TTA ATG GCA TTT TCC TGG TAC **CTT** AAT CGG TAC-3′; K8D-P9S-H10V-R58K, 5′-CGT CTA GAT AAA AGA AAT TCT GTT CGG GAT GCT TAT ATT GCC **GAT AGT GTA** AAC TGT-3′ K8D-P9S-R58K-V59G, 5′-CG AAG CTT TTA ATG GCA TTT TCC TGG **GGT CTT** AAT CGG TAC-3′; K8D-P9S-R58K-P60G, 5′-CG AAG CTT TTA ATG GCA TTT TCC **GGT** TAC **CTT** AAT CGG TAC-3′. Mutants K8D, K8A, K8G and K8Q were created by using pVT102U/α-BmK M1 as template along with primer 2. Mutant K8D-P9S was created by using pVT102U/α-K8D as template along with primer 2. Mutants R58K and R58K-P60G were created by using pVT102U/α-BmK M1 as template along with primer 1. Mutant K8D-P9S-R58K was created by using pVT102U/α-K8D-P9S as template along with primer 1. Mutants K8D-P9S-R58K-V59G and K8D-P9S-R58K-P60G were created by using pVT102U/α-K8D-P9S-R58K as template along with primer 1. Mutant K8D-P9S-H10V-R58K was created by using pVT102U/α-K8D-P9S-R58K as template along with primer 2.

Expression and purification of BmK M1 mutants

The mutated cDNA gene was inserted into the plasmid and then expressed in *S. cerevisiae* S-78 yeast cells.[22,23] Purification of the expressed mutants was carried out by two successive chromatography steps. First, cationic-exchange chromatography was applied using a CM32-cellulose column (Whatman, England). The eluted fraction containing the target protein was further purified by using a Sephasil® peptide C18 column on an ÄKTA Purifier chromatography system (Amersham Biosciences, Sweden). The purification procedure has been described elsewhere.[23] Final purified samples were examined by ESI mass spectrometry using an API 3000 triple quadrupole mass spectrometer (Perkin-Elmer Sciex Instruments, Canada) and a Thermofinnigan Deca XP ion-trap LC/MS.

Bioassay

LD_{50} values on mice (male, specified pathogen-free level, 18–22 g of body weight) of the BmK M1 mutants were determined according to the method of Meier & Theakston.[36] Unmodified rBmK M1 and 0.9% (w/v) NaCl were used as a positive and a negative control, respectively. Various doses of mutants were dissolved in 0.9% (w/v) NaCl and injected into the mice through the tail vein. Body weights, survival times (times between injection and death), reaction and doses were recorded.

Electrophysiological recordings and analysis

For the expression in *X. laevis* oocytes, the $Na_v1.5$ (human heart) and β_1 genes were subcloned into pSP64T.[37] For *in vitro* transcription, $Na_v1.5$/pSP64T was first linearized with XbaI and β_1/pSP64T with EcoRI. Next, capped cRNAs were synthesized using the SP6 mMESSAGE-mMACHINE transcription kit (Ambion, USA). The para/pGH19-13-5 vector, tipE/pGH19 vector and $Na_v1.2$/pLCT1 vector were linearized with NotI and transcribed with the T7 mMESSAGE-mMACHINE kit (Ambion, USA).[5,38,39]

The harvesting of oocytes from female *X. laevis* frogs and RNA injection was as described.[40] The solution used for incubating the oocytes (ND96) contained 96 mM NaCl, 2 mM KCl, 198 mM $CaCl_2$, 2 mM $MgCl_2$ and 5 mM Hepes (pH 7.4), supplemented with 50 mg l^{-1} gentamycin sulphate and 90 mg l^{-1} theophyllin.

Two-electrode voltage-clamp recordings were performed at room temperature (18 °C −22 °C) using a GeneClamp 500 amplifier (Axon instruments, USA) controlled by a pClamp data acquisition system (Axon instruments, USA). Voltage and current electrodes were filled with 3 M KCl. Resistances of both electrodes were kept as low as possible (<0.5 MΩ). The bath solution composition was 96 mM NaCl, 2 mM KCl, 1.8 mM $CaCl_2$, 2 mM $MgCl_2$ and 5 mM Hepes (pH 7.4). Using a four-pole low-pass Bessel filter, currents were filtered at 1 kHz and sampled at 5 kHz. Leak subtraction was performed using a −P/2 protocol. Whole-cell currents from oocytes were recorded two to four days after injection. Current traces (see also Figure 2) were evoked by depolarisations ranging from −20 mV to 10 mV depending on the VGSC in order to measure at the voltage of maximal Na^+ influx (determined in the current–voltage relationship). The holding potential was −90 mV.

The degree of fast inactivation was assayed by measuring the $I_{10\ ms}/I_{peak}$ ratio, which gives an estimate of the probability for the channels not to be inactivated after 10 ms.[41] Depending on the VGSC, a test voltage was chosen so that $I_{10\ ms}/I_{peak}$ was close to zero under control conditions. The $I_{10\ ms}/I_{peak}$ ratio was measured at the same test voltage after addition of the toxin. Toxin-induced removal of fast inactivation was measured by plotting $I_{10\ ms}/I_{peak}$ as a function of toxin concentrations. A Boltzman sigmoidal fit of these data resulted in the EC_{50} values presented in Table 1. Curve manipulations were performed using pClamp8 (Axon instruments, USA) and Origin software (Microcal, USA).

CD measurements

Samples used for CD analyses were dissolved in 25 mM Tris–HCl (pH 8.0) at a concentration of 1.0 mg/ml. The measurements were performed from 250 nm to 200 nm at room temperature in a 1 mm path-length quartz cell with a Jasco J-720 spectropolarimeter. All data resulted from averaging four scans. The final spectrum was corrected by subtracting the corresponding base-line spectrum and was smoothed by the instrument's software.

Crystal structural determination

Crystallization

Among 11 mutants, eight mutants with high purity were used for crystallization. Two mutants (K8D and K8Q) have been reported before.[17,26] The mutants were prepared at a concentration of 20 mg/ml in water for crystallization. Crystallizing conditions were screened in hanging-drop, vapour-diffusion experiments with drops equilibrated against 500 µl of reservoir solution at room temperature. Eight crystals suitable for X-ray diffraction analysis were obtained. Detailed crystallizing conditions of the eight mutants are 30% (w/v) PEG8000, 0.1 M sodium cacodylate (pH 6.5) and 0.2 M ammonium sulphate for K8A, K8Q, K8D-P9S-R58K and K8D-P9S-R58K-P60G; 1.5 M sodium phosphate (pH 6.0) for K8D and K8D-P9S; 30% (w/v) PEG4000, 0.1 M Tris–HCl (pH 8.5) and 0.2 M sodium acetate for K8G; 30% (w/v) PEG4000, 0.1 M Tris–HCl (pH 8.5) and 0.2 M lithium sulphate for K8D-P9S-R58K-V59G.

Data collection and processing

X-ray diffraction data of K8D and K8D-P9S were collected at room temperature using synchrotron radiation ($\lambda = 1.0$ Å) on an ADSC Quantum 4 CCD detector at the beam line BL18B of the Photon Factory in Tsukuba, Japan. Diffraction data of K8D-P9S-R58K-P60G and K8D-P9S-R58K-V59G were collected using synchrotron radiation ($\lambda = 0.9$ Å) on a Mar165 CCD detector at BSRF in Beijing, China. Diffraction data of K8Q, K8G, K8A and K8D-P9S-R58K were collected using CuKα radiation ($\lambda = 1.5418$ Å) on a Mar345 image-plate detector, an Raxis VI++ image-plate detector and a Bruker AXS Smart2000 CCD detector, respectively. The diffraction data were processed and analysed by using MOSFLM/SCALA[42] and Proteum™ (Table 2).

Structural solution and refinement

All structures of the BmK M1 mutants were solved by molecular replacement using the program AMoRe.[43] The structure of the native BmK M1 (PDB, 1sn1)[17] was used as an initial model. The unique solutions for the rotation and translation searches were obvious, exhibiting initial CC and *R* factor values of about 0.60 and 0.40, respectively, after rigid-body refinement.

The initial structures of BmK M1 mutants were refined with CNS[44] and the models were rebuilt with O.[45] During the model rebuilding, all mutated residues were not substituted with the target amino acids until they were confirmed as being correct in an omit $F_o - F_c$ map. All the refinements were performed using iterative rounds of positional and individual *B* factor refinement, as well as the addition of solvent molecules with 8–10% of the data randomly excluded and used as a cross-validation test using the free *R* factor.[46]

Protein Data Bank accession codes

The coordinates and structural factors of the eight mutants of BmK M1 have been deposited to the RCSB PDB with accession numbers 1ZU3, 1ZVE, 1T7A, 1T7B, 1ZUG, 1ZUT, 1ZYV and 1ZYW, respectively.

Acknowledgements

The project was supported by NNSF (30370320), the Ministry of Science and Technology of China (2002BA711A13, G19990756), grant G.0081.02 (F.W.O. Vlaanderen), Flanders/People's Republic of China Bilateral grant BIL00/06 and the Chinese Academy of Sciences (KSCX1-SW-17, KSCXZ-SW-322).

We thank Martin S. Williamson, IACR-Rothamsted, UK for the para and tipE clone; A. L. Goldin, University of California, Irvine, USA for $Na_v1.2$; R.G. Kallen, University of Pennsylvania, Philadelphia, USA for $Na_v1.5$; S. H. Heinemann, Friedrich-Schiller-Universität Jena, Germany for the β_1 subunit; and Stefaan Sansen for helpful discussions.

References

1. Yu, F. H., Westenbroek, R. E., Silos-Santiago, I., McCormick, K. A., Lawson, D., Ge, P. *et al*. (2003). Sodium channel β4, a new disulfide-linked auxiliary subunit with similarity to β2. *J. Neurosci.* **23**, 7577–7585.
2. Denac, H., Mevissen, M. & Scholtysik, G. (2000). Structure, function and pharmacology of voltage-gated sodium channels. *Naunyn Schmiedebergs Arch. Pharmacol.* **362**, 453–479.
3. Catterall, W. A. (2000). From ionic currents to molecular mechanisms: the structure and function of voltage-gated sodium channels. *Neuron*, **26**, 13–25.
4. Goldin, A. L., Barchi, R. L., Caldwell, J. H., Hofmann, F., Howe, J. R., Hunter, J. C. *et al*. (2000). Nomenclature of voltage-gated sodium channels. *Neuron*, **28**, 365–368.
5. Warmke, J. W., Reenan, R. A., Wang, P., Qian, S., Arena, J. P., Wang, J. *et al*. (1997). Functional expression of *Drosophila* para sodium channels. Modulation by the membrane protein TipE and toxin pharmacology. *J. Gen. Physiol.* **110**, 119–133.
6. Zlotkin, E. (1999). The insect voltage-gated sodium channel as target of insecticides. *Annu. Rev. Entomol.* **44**, 429–455.
7. Wang, S. Y. & Wang, G. K. (2003). Voltage-gated sodium channels as primary targets of diverse lipid-soluble neurotoxins. *Cell. Signal.* **15**, 151–159.
8. Possani, L. D., Becerril, B., Delepierre, M. & Tytgat, J. (1999). Scorpion toxins specific for Na^+-channels. *Eur. J. Biochem.* **264**, 287–300.
9. Bosmans, F., Aneiros, A. & Tytgat, J. (2002). The sea

anemone *Bunodosoma granulifera* contains surprisingly efficacious and potent insect-selective toxins. *FEBS Letters*, **532**, 131–134.
10. Grolleau, F., Stankiewicz, M., Birinyi-Strachan, L., Wang, X. H., Nicholson, G. M., Pelhate, M. & Lapied, B. (2001). Electrophysiological analysis of the neurotoxic action of a funnel-web spider toxin, delta-atracotoxin-HV1a, on insect voltage-gated Na^+ channels. *J. Expt. Biol.* **204**, 711–721.
11. Seibert, A. L., Liu, J., Hanck, D. A. & Blumenthal, K. M. (2004). Role of Asn-16 and Ser-19 in anthopleurin B binding. Implications for the electrostatic nature of Na(V) site 3. *Biochemistry*, **43**, 7082–7089.
12. Gordon, D., Martin-Eauclaire, M. F., Cestele, S., Kopeyan, C., Carlier, E., Khalifa, R. B. *et al*. (1996). Scorpion toxins affecting sodium current inactivation bind to distinct homologous receptor sites on rat brain and insect sodium channels. *J. Biol. Chem.* **271**, 8034–8045.
13. Gordon, D., Savarin, P., Gurevitz, M. & Zinn-Justin, S. (1998). Functional anatomy of scorpion toxins affecting sodium channels. *J. Toxicol. Toxin Rev.* **17**, 131–159.
14. Housset, D., Habersetzer-Rochat, C., Astier, J. P. & Fontecilla-Camps, J. C. (1994). Crystal structure of toxin II from the scorpion *Androctonus australis* Hector refined at 1.3 Å resolution. *J. Mol. Biol.* **238**, 88–103.
15. Li, H. M., Wang, D. C., Zeng, Z. H., Jin, L. & Hu, R. Q. (1996). Crystal structure of an acidic neurotoxin from scorpion *Buthus martensii* Karsch at 1.85 Å resolution. *J. Mol. Biol.* **261**, 415–431.
16. Tugarinov, V., Kustanovich, I., Zilberberg, N., Gurevitz, M. & Anglister, J. (1997). Solution structures of a highly insecticidal recombinant scorpion α-toxin and a mutant with increased activity. *Biochemistry*, **36**, 2414–2424.
17. He, X. L., Li, H. M., Zeng, Z. H., Liu, X. Q., Wang, M. & Wang, D. C. (1999). Crystal structures of two alpha-like scorpion toxins: non-proline *cis* peptide bonds and implications for new binding site selectivity on the sodium channel. *J. Mol. Biol.* **292**, 125–135.
18. Krimm, I., Gilles, N., Sautiere, P., Stankiewicz, M., Pelhate, M., Gordon, D. & Lancelin, J. M. (1999). NMR structures and activity of a novel α-like toxin from the scorpion *Leiurus quinquestriatus hebraeus*. *J. Mol. Biol.* **285**, 1749–1763.
19. Goudet, C., Huys, I., Clynen, E., Schoofs, L., Wang, D. C., Waelkens, E. & Tytgat, J. (2001). Electrophysiological characterization of BmK M1, an alpha-like toxin from *Buthus martensi* Karsch venom. *FEBS Letters*, **495**, 61–65.
20. Goudet, C., Chi, C. W. & Tytgat, J. (2002). An overview of toxins and genes from the venom of the Asian scorpion *Buthus martensi* Karsch. *Toxicon*, **40**, 1239–1258.
21. Xiong, Y. M., Ling, M. H., Wang, D. C. & Chi, C. W. (1997). The cDNA and genomic DNA sequences of a mammalian neurotoxin from the scorpion *Buthus martensii* Karsch. *Toxicon*, **35**, 1025–1031.
22. Shao, F., Xiong, Y. M., Zhu, R. H., Ling, M. H., Chi, C. W. & Wang, D. C. (1999). Expression and purification of the BmK M1 neurotoxin from the scorpion *Buthus martensii* Karsch. *Protein Expr. Purif.* **17**, 358–365.
23. Sun, Y. M., Bosmans, F., Zhu, R. H., Goudet, C., Xiong, Y. M., Tytgat, J. & Wang, D. C. (2003). Importance of the conserved aromatic residues in the scorpion α-like toxin BmK M1: the hydrophobic surface region revisited. *J. Biol. Chem.* **278**, 24125–24131.
24. Wang, C. G., Gilles, N., Hamon, A., Le Gall, F., Stankiewicz, M., Pelhate, M. *et al*. (2003). Exploration of the functional site of a scorpion α-like toxin by site-directed mutagenesis. *Biochemistry*, **42**, 4699–4708.
25. Liu, L. H., Bosmans, F., Maertens, C., Zhu, R. H., Wang, D. C. & Tytgat, J. (2005). Molecular basis of the mammalian potency of the scorpion α-like toxin, BmK M1. *FASEB J.* **19**(6), 594–596.
26. Guan, R. J., Xiang, Y., He, X. L., Wang, C. G., Wang, M., Zhang, Y. *et al*. (2004). Structural mechanism governing *cis* and *trans* isomeric states and an intramolecular switch for *cis*/*trans* isomerization of a non-proline peptide bond observed in crystal structures of scorpion toxins. *J. Mol. Biol.* **341**, 1189–1204.
27. Karbat, I., Frolow, F., Froy, O., Gilles, N., Cohen, L., Turkov, M. *et al*. (2004). Molecular basis of the high insecticidal potency of scorpion α-toxins. *J. Biol. Chem.* **279**, 31679–31686.
28. Rochat, H., Bernard, P. & Couraud, F. (1979). Scorpion toxins: chemistry and mode of action. *Advan. Cytopharmacol.* **3**, 325–334.
29. Catterall, W. A., Ray, R. & Morrow, C. S. (1976). Membrane potential dependent binding of scorpion toxin to action potential Na^+ ionophore. *Proc. Natl Acad. Sci. USA*, **73**, 2682–2686.
30. Catterall, W. A. (1977). Membrane potential-dependent binding of scorpion toxin to the action potential Na^+ ionophore. Studies with a toxin derivative prepared by lactoperoxidase-catalyzed iodination. *J. Biol. Chem.* **252**, 8660–8668.
31. Catterall, W. A. (1979). Binding of scorpion toxin to receptor sites associated with sodium channels in frog muscle. Correlation of voltage-dependent binding with activation. *J. Gen. Physiol.* **74**, 375–391.
32. Benkhadir, K., Kharrat, R., Cestele, S., Mosbah, A., Rochat, H., El Ayeb, M. & Karoui, H. (2004). Molecular cloning and functional expression of the alpha-scorpion toxin BotIII: pivotal role of the C-terminal region for its interaction with voltage-dependent sodium channels. *Peptides*, **25**, 151–161.
33. Gurevitz, M., Gordon, D., Ben-Natan, S., Turkov, M. & Froy, O. (2001). Diversification of neurotoxins by C-tail 'wiggling': a scorpion recipe for survival. *FASEB J.* **15**, 1201–1205.
34. Legros, C., Ceard, B., Vacher, H., Marchot, P., Bougis, P. E. & Martin-Eauclaire, M. F. (2005). Expression of the standard scorpion α-toxin AaH II and AaH II mutants leading to the identification of some key bioactive elements. *Biochim. Biophys. Acta*, **1723**, 91–99.
35. Zilberberg, N., Froy, O., Loret, E., Cestele, S., Arad, D., Gordon, D. & Gurevitz, M. (1997). Identification of structural elements of a scorpion α-neurotoxin important for receptor site recognition. *J. Biol. Chem.* **272**, 14810–14816.
36. Meier, J. & Theakston, R. D. (1986). Approximate LD50 determinations of snake venoms using eight to ten experimental animals. *Toxicon*, **24**, 395–401.
37. Gellens, M. E., George, A. L., Jr, Chen, L. Q., Chahine, M., Horn, R., Barchi, R. L. & Kallen, R. G. (1992). Primary structure and functional expression of the human cardiac tetrodotoxin-insensitive voltage-dependent sodium channel. *Proc. Natl Acad. Sci. USA*, **89**, 554–558.
38. Feng, G., Deak, P., Chopra, M. & Hall, L. M. (1995). Cloning and functional analysis of TipE, a novel membrane protein that enhances *Drosophila* para sodium channel function. *Cell*, **82**, 1001–1011.
39. Noda, M., Ikeda, T., Kayano, T., Suzuki, H.,

Takeshima, H., Kurasaki, M. *et al*. (1986). Existence of distinct sodium channel messenger RNAs in rat brain. *Nature*, **320**, 188–192.
40. Liman, E. R., Tytgat, J. & Hess, P. (1992). Subunit stoichiometry of a mammalian K^+ channel determined by construction of multimeric cDNAs. *Neuron*, **9**, 861–871.
41. Chen, H., Lu, S., Leipold, E., Gordon, D., Hansel, A. & Heinemann, S. H. (2002). Differential sensitivity of sodium channels from the central and peripheral nervous system to the scorpion toxins Lqh-2 and Lqh-3. *Eur. J. Neurosci.* **16**, 767–770.
42. Collaborative Computational Project Number 4 (1994). The CCP4 suite: programs for protein crystallography. *Acta Crystallog. sect. D*, **50**, 760–763.
43. Navaza, J. (1994). AMoRe–an automated package for molecular replacement. *Acta Crystallog. sect. A*, **50**, 157–163.
44. Brunger, A. T., Adams, P. D., Clore, G. M., DeLano, W. L., Gros, P., Grosse-Kunstleve, R. W. *et al*. (1998). Crystallography & NMR system: a new software suite for macromolecular structure determination. *Acta Crystallog. sect. D*, **54**, 905–921.
45. Jones, T. A., Zou, J. Y., Cowan, S. W. & Kjeldgaard, M. (1991). Improved methods for building protein models in electron density maps and the location of errors in these models. *Acta Crystallog. sect. A*, **47**, 110–119.
46. Brünger, A. T. (1992). Free *R*-value: a novel statistical quantify for assessing the accuracy of crystal structures. *Nature*, **355**, 472–475.

Edited by I. B. Holland

(Received 14 July 2005; received in revised form 26 August 2005; accepted 26 August 2005)
Available online 22 September 2005